IEEE Access
Multidisciplinary | Rapid Review | Open Access Journal

Received March 14, 2019, accepted April 1, 2019, date of current version April 22, 2019.

Digital Object Identifier 10.1109/ACCESS.2019.2910592

Interference Analysis and Filter Parameters Optimization for Uplink Asynchronous F-OFDM Systems

MEIJIE YANG, YUEYUN CHEN, AND LIPING DU
University of Science and Technology Beijing, Beijing 100083, China

Corresponding author: Yueyun Chen (chenyy@ustb.edu.cn)

This work was supported by the National Science and Technology Major Project under Grant 2017ZX03001021-005.

ABSTRACT Filtered-orthogonal frequency division multiplexing (F-OFDM) is a candidate for 5G new waveform, which has flexible numerologies to support various scenarios and can combat interference of multi-users effectively with filters. However, although longer filter length and higher roll-off factor can suppress out of band radiation, inter-symbol interference (ISI) and inter-carrier interference (ICI) will increase at the same time. Meanwhile, the wider guard band reduce inter-user interference (IUI) at the cost of higher spectrum occupancy. To meet target bit error rate (BER) requirements of all users and maximize the spectrum efficiency, a filter parameter and guard bandwidth optimization model was proposed to design related parameters dynamically for uplink asynchronous F-OFDM system, where users are allocated with different numerologies. We present a detailed theoretical derivation on ISI, ICI, and IUI for BER calculation, and the theoretical derivation of IUI in multi-user scenario with different subcarrier spacing between users is first presented. The formulated problem is proved to be a non-convex NP hard problem and Imperialist Competitive Algorithm (ICA) is applied for a desirable solution. The simulation results show that the theoretical derivations are valid and the proposed filter parameter and guard bandwidth optimization model can achieve higher spectrum efficiency than the fixed filter parameters in F-OFDM while outperforms traditional OFDM.

INDEX TERMS Filtered-orthogonal frequency division multiplexing (F-OFDM), interference analysis, spectrum efficiency, multi-numerologies.

I. INTRODUCTION

Upcoming 5G wireless communication will provide more scenarios, including ultra-reliable and low-latency communications (uRLLC), enhanced mobile broadband (eMBB) and massive machine type communications (mMTC) [1], to fulfill less than 1ms latency, 20 Gb/s peak data rate and $10^6/km^2$ device density targets in future daily communications [2], [3]. With the appearance of service diversity and the increase of device density, data traffic requirement presents a tendency of rapid rise undeniably [4]. However, the shortage of spectrum resources and the inflexibility of the current orthogonal frequency division multiplexing (OFDM) waveform become bottlenecks of future communication [5].

OFDM is sensitive to the frequency offset, we have to achieve stringent synchronization using signaling and cyclic prefix (CP) in time domain at the cost of reducing time efficiency [6]. Besides, 10% of the overall bandwidth is reserved as guard band under the LTE specifications to suppress serious out of band leakage [4], this characteristic also limits the flexibility of sub-carrier spacing configuration, because multi-user interference will be enlarged when different parameters applied between adjacent users. These two factors, to a great extent, waste rare time and frequency resource, respectively.

To overcome these disadvantages and to meet the 5G demand of multi-numerologies coexistence, bandwidth extension, frequency-domain and time-domain well localization, MIMO friendliness and high-order modulation [5], several new waveforms are proposed recently. The main candidates of 5G waveforms are roughly include sub-band filtering based multicarrier modulation and pulse shaping based multicarrier modulation [7], [8]. Filter bank multicarrier (FBMC) [9] and generalized frequency division

The associate editor coordinating the review of this manuscript and approving it for publication was Yunlong Cai.

multiplexing (GFDM) [10] are modulations based on pulse shaping, while universal-filtered OFDM (UFMC) [11], windowed-OFDM (W-OFDM) [12] and F-OFDM [13], [14] are waveforms based on sub-band filtering. The filters in FBMC are used on each target subcarrier to achieve better localization in frequency domain [15]-[17], and the absence of the CP leads to high spectral efficiency [17]. However, due to the narrow bandwidth of filters used in FBMC, a long tailing in time domain is unavoidable which introduces additional computational complexity. GFDM adopts a tail biting technique to shorten the cyclic prefix, which may get better time-domain efficiency compared with FBMC [7]. Besides, GFDM also has better spectrum efficiency compared with waveforms based on sub-band filtering, just like FBMC [18]. Nevertheless, it needs sophisticated interference cancellation [10], [19]. UFMC is zero padding (ZP)-based and uses short sub-band filters to minimize trailing in time-domain. But the constraints on filter length limited the OOB suppression performance [20]. Only unified subcarrier spacing is considered also limits the flexibility of UFMC. The W-OFDM configures simple time domain window and the enhancement of time-domain efficiency totally depends on shorten effective CP length, which at the expense of sacrifice performance against multipath interference [5].

F-OFDM is also an OFDM-based waveform and delivers extraordinary benefits. Firstly, its spectrums are divided into a series of contiguous sub-bands and the same filtering operation is performed on the granularity of each user [14], it possesses better OOB suppression and spectrum efficiency compared with other waveforms based on sub-band filtering [5]. Meanwhile, although subcarrier filtering waveforms like FBMC and GFDM has better frequency localization, the high complexity at the receiver remains as a problem [21], then, lower implementation complexity becomes another advantage of F-OFDM in this respect. Secondly, the sub-band filtering operation helps F-OFDM realize asynchronous transmission between users and non-contiguous spectrum is highly utilized. A lot of time and spectrum resources are saved to deal with resource scarcity [22]. Thirdly, tailored numerology for different services is more suitable for 5G requirements. Choosing a proper sub-carrier spacing, filter length and roll-off parameters significantly improve the system performance. Just same as traditional OFDM, multipath interference is conquered by using CP, which also prevent from introducing too much ISI from adjacent symbols. Flexible CP length can be used in F-OFDM to serve different kinds of services reasonably [23], [24]. Overall, F-OFDM is a competitive waveform for 5G system.

In traditional OFDM system, ICI caused by Doppler spread has severely influence on signal to interference plus noise ratio (SINR), BER and system capacity [25]. F-OFDM has the similar characteristic with OFDM, but it put slightly different. Unlike OFDM, F-OFDM system could employ different sub-carrier spacing [26], [27]. In mobile scenario, wider sub-carrier spacing is applied to weaken Doppler spread. ICI and ISI caused by insufficient CP is another issue, which would dramatically degrade the performance of the whole system [28]. SINR of CP insufficient system has been analyzed in OFDM and UFMC, and corresponding interference mitigation method has been proposed [22]. Because UFMC and F-OFDM are all based on sub-band filtering, therefore the interference analysis in UFMC [29], [30] also has significant value for F-OFDM. In multi-user F-OFDM system, IUI is unavoidable when multi-user coexistence, and several papers have studied the influence of this kind of interference [26]-[28], [31]. The only drawback is that different carrier spacing is not taken into consideration which would not describe the characteristic of F-OFDM completely. If adjacent users employ different carrier spacing, it is better to consider whether guard bands are needed [32]. Although the bit error rate affected by the relative position between users has been analyzed, quantitative analysis still needed. As we all know, asynchronous transmission represents that F-OFDM is flexible enough to deal with services in different scenarios, obvious performance loss has been observed when implementing asynchronous transmission in OFDM while F-OFDM maintain robustness [22], [23]. But field trial and qualitative analysis are not enough; the results of theoretical analysis will be more convincing especially for the multi-numerologies scenario. F-OFDM typically adopts FIR filter, different performances of diverse FIR filter are obtained through previous studies [13], [14], [33]. Actually, different users may need filters with different parameters, including filter length and roll-off factor [11]. How to choose superior parameters to maximize the spectrum efficiency in F-OFDM is still a problem to be solved. Overall, the target is to design proper FIR filter parameters to suppress out of band radiation while guarantee a suitable user BER in order to enhance system capacity and further promote spectrum efficiency.

Compared with former literatures, this paper has the following contributions:

(1) Filter parameters and guard bandwidth optimization model is proposed to maximize frequency spectrum efficiency. We configure filter parameters flexibly for interference minimization which subject to theoretical BER of all users to ensure service demands. The proposed model which is non-convex NP hard is solved by ICA to get optimized solutions.

(2) The theoretical derivations of interference and BER in multi-user multi-numerologies F-OFDM system are presented. The ISI and ICI are caused by insufficient CP length while IUI which is first theoretical derived in this paper is caused by asynchronous transmission and different parameters configuration of different users. It has been demonstrated that different parameters configuration could introduce different SINR to the system, and as a result, BER will be distinct. Poor BER performance cannot satisfy the normal communication needs for users which emphasize the importance to optimize the parameters configured.

(3) Simulation results show that the results of theoretical deduction is consistent with that of Monte Carlo simulations

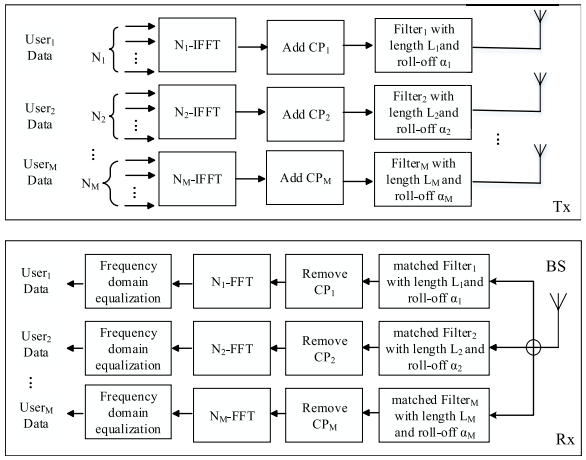

FIGURE 1. Transceiver structure of uplink F-OFDM system.

and the F-OFDM with parameter optimization get better frequency spectrum efficiency compared with fixed filter parameters in F-OFDM and OFDM while maintain enough flexibility.

The remainder of this paper is organized as follows. We describe the system model of F-OFDM and propose a filter parameters and guard bandwidth optimization model in section II. Next, Detailed theoretical derivation of SINR in dynamic parameters multi users F-OFDM system is present in section III. Model Analysis and problem solving is given in section IV. Section V shows the simulation results of related researches. Finally, we draw a conclusion in section VI.

II. SYSTEM MODEL

A. TRANSCEIVER STRUCTURE

The transceiver structure of the uplink F-OFDM with the proposed filter parameter and guard bandwidth optimization scheme is shown in Fig. 1. The filter parameters which correspond to different numerologies of various users are optimized dynamically. Filter parameter optimization helps to depress multi-user interference from the side-lobes of adjacent users while maintaining the ISI and ICI from the current user itself under an acceptable level. The system takes frequency selective flat fading channel into consideration and the filters employ Windowed-Sinc method.

There are U users available simultaneously and each user has N_u $(u = 1, 2, \cdots, U)$ subcarriers. The Fast Fourier transform (FFT) length, inverse Fast Fourier transform (IFFT) length and CP length of each user are N_{FFT_u}, N_{IFFT_u} and N_{CP_u} respectively. The transmitted data in the n_{th} subcarrier of user u is $d_{u,n}$, and the g_{th} signal sample of user u after modulation in time domain is given as

$$x_u(g) = \sum_{i=1}^{I} x_{i,u}\left(\left[g - iN_{FFT_u} - (i+1)N_{CP_u}\right]_{\bmod N_{FFT_u}}\right) \tag{1}$$

where $x_{i,u}(s) = \sum_{n=n_u-1}^{n_u+N_u-1} d_{u,n} e^{\frac{j2\pi ns}{N_{FFT_u}}}$, $-N_{CP_u} \le s < N_{FFT_u}$, and n_u is the location of the first sub-carrier of user u.

Before the modulated signal transmitted, a FIR filter is employed to suppress the out of band radiation in order to mitigate the interference from other users. High degree decoupling between users is also obtained by using filters for asynchronous transmission. Signal of user u after filtering is written as $s_u(g) = x_u(g) * f_u(g)$, where $*$ represents the convolution operation and the length of filter f_u usually less than half of the symbol, because longer filter length will cause more serious ISI and ICI if CP is insufficient.

In the uplink F-OFDM system, after a frequency selective flat fading channel, the received signal of user u is given by

$$y_u(g) = x_u(g) * f_u(g) * h_u(g) + \sum_{\substack{u'=1 \\ u' \neq u}}^{U} x_{u'}(g - \tau_{u'}) * f_{u'}(g) * h_{u'}(g) + z_u(g) \tag{2}$$

where τ_u is time delay and corresponds to asynchronous transmission, h_u represents impulse response of multipath channel experienced by user u.

Rayleigh fading model is considered and multipath components are uncorrelated. z_u is complex additive white Gauss noise (AWGN) of user u with zero mean and variance σ_u^2. Receiving filter f_u^* is a match filter applied to distinguish users, and the filtered signal at receiver is $R_u(g) = y_u(g) * f_u^*(g)$.

Eventually, the signals are processed by FFT operation and other followed operations in frequency domain, and zero-force (ZF) channel equalization is adopted in this paper.

B. FILTER DESIGN CRITERIA

A Windowed-Sinc method [13], [14] typical expresses as $f_u(n) = \omega_u(n) \times f_{ideal,u}(n)$, where $f_{ideal,u}$ is an ideal lineal phase band-pass filter corresponding to sinc function in time domain, which is infinite and need to be cut off. ω_u is a window function with limited length in time domain, and some typical windows such as Hamming Window, Hanning Window, Blackman Window and Chebyshev Window, etc. are usually considered in F-OFDM sub-band filter design. We utilize Kaiser-Basel Window to construct a FIR filter. Kaiser-Basel Window has an advantage over the other kind of FIR filters on its flexible roll-off parameter configuration. Kaiser-Basel Window function is [34-36]

$$\omega_u(n) = \frac{J_0\left(\alpha_u\sqrt{1 - \left(\frac{2n}{L_{f,u}-1} - 1\right)^2}\right)}{J_0(\alpha_u)}, 0 \le n \le L_{f,u} \tag{3}$$

where J_0 is zero-order modified Bessel function, $L_{f,u}$ is filter length of user u. For the same user, transmit filter length equals to receive filter length for simplicity. α_u is roll-off coefficient which controls the shape of the window, as it gets smaller, the main lobe becomes narrow, but the amplitude of side lobe increases. $L_{f,u}$ has a similar situation, the width

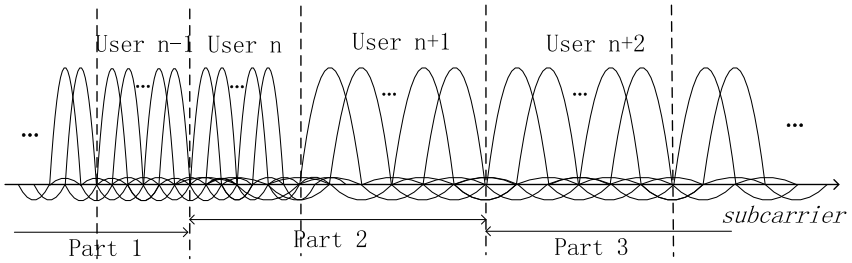

FIGURE 2. Users spectrum arrangement in multi-user system.

of the main lobe decreases as it grows but time domain ISI becomes more serious.

Filter design criterias in [33] explain that higher order filter results in better performance. It may be correct when we only take multi-user interference into account, because higher order filter possesses longer filter length, and have better frequency localization. However, it may produce more ISI and ICI to the target user in the above case. Meanwhile, as the value of α_u becomes smaller, the time localization characteristic turns out to be undesirable, therefore it could produce serious interference between adjacent symbols.

It is simple to get the IUI by overlapping signals in frequency domain as [11]. However, simply considering side-lobe attenuation is not applicable in multi-numerologies asynchronous systems because different symbol length leads to non-orthogonality in time domain between users which introducing extra interference. Besides, ISI and ICI cannot be reflected, so we need a more comprehensive analysis to obtain accurate BER performances.

Accordingly, we have to balance the multi-user interference and self-interference at the same time, then the system achieves optimal performance while ensuring the needs of all users.

C. PROPOSED FILTER PARAMETERS AND GUARD BAND WIDTH OPTIMIZATION

The coexistence of multiple numerologies reflects highly flexible of F-OFDM system. Wider subcarrier spacing has short TTI and is more suitable for real-time service, but that also contributes to the occurrence of more serious multi-user interference when coexistence with other kinds of subcarrier spacings.

The scheme assumes that users with different subcarrier spacing have same CP length in this paper. CP length and subcarrier spacing are directly related with spectrum utilization and when same subcarrier spacing is employed, multi-user interference is small just as Fig. 5 and Fig. 9 show. Users with same subcarrier spacing are arranged together, and then the number of intersection points of different subcarrier spacing is relatively small. Consequently, the number of guard band will be reduced in multi-user scenario. And for users with same subcarrier spacing, the filter parameters should be reasonable to depress ISI and asynchronous interference. The subcarrier spacing is set to be $\Delta f_u = 15 \times 2^k KHz$, $k = 0, 1, 2, \cdots$ for user u.

As Fig. 2 shows, users in the first and third part contain same subcarrier spacing respectively, and the second part represents the adjacent edge users of different subcarrier spacing. In the uplink system, IUI exists during transmission and subcarrier spacing of each user has been determined before transmission. The related parameters are guard bandwidth and filter parameters they employed. Parameters for maximizing spectrum efficiency are achieved as followed

$$\begin{aligned} \max_{\{\{\alpha\},\{L_f\},\{B_g\}\}} \quad & \frac{\sum_{u=1}^{U} \sum_{n=n_u-1}^{N_u+n_u-1} C_{u,n}}{\sum_{u=1}^{U} B_u + \sum_{i=1}^{U-1} B_{g,i}} \\ s.t. \quad & \alpha_i > 0 \\ & L_{fu} \leq 0.5 N_u \\ & P_{e,u} \leq P_{e,u,t} \end{aligned} \tag{4}$$

where $\{\alpha\}\{L_f\}\{B_g\}$ are solution sets of above-mentioned model, α is filter roll-off, L_f represents filter length and $B_{g,i}$ is the guard bandwidth between user i and $i+1$. $C_{u,n}$ represents the capacity of user u in subcarrier n, and B_u is the bandwidth of user u.

The F-OFDM filter length is less than half of the symbol length in general. Δf_k is the corresponding subcarrier spacing. $P_{e,u}$ is BER in practice and $P_{e,u,t}$ is BER threshold for each user.

III. INTERFERENCE ANALYSIS

In a multi user system, poor side-lobe attenuation causes IUI between users, however, rapid side-lobe attenuation, which at the expense of longer filter length and lower value of roll-off factor, may further influence the ISI and ICI produced by target users themselves. Interference caused by diverse numerologies, notably subcarrier spacing, is especially worth studying. Asynchronous transmission also deserves close attention for the sake of synchronous relaxation.

A. DESIRED SIGNAL FOR CP INSUFFICIENT

A lot of related work has been done for OFDM [38], [39], however, it is not enough for F-OFDM. Besides channel impulse responds, filter impulse responds should also be

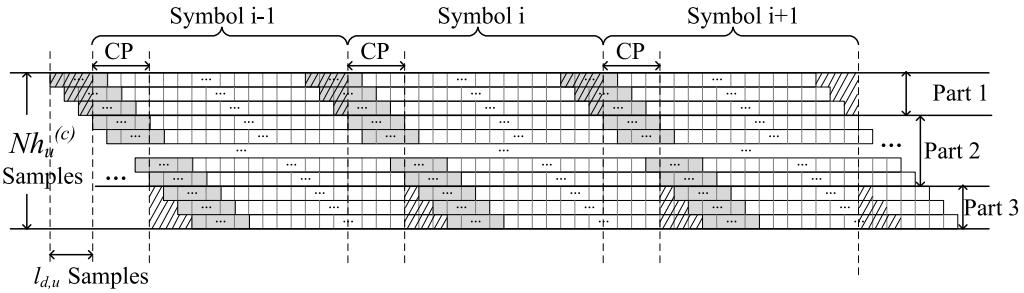

FIGURE 3. The effect of filters and channel.

taken into consideration. For the convenience and simplicity of the derivation, we combine the effect of the two mentioned above. $h_u^{(c)} = f_u * h_u * f_u{}^*$, where $h_u^{(c)}$ is the convolution of filter and channel tap gain in time domain, and the length of $h_u^{(c)}$ is $Nh_u^{(c)} = Nh_u + L_{f,u} + L_{f^*,u} - 2$, $L_{f^*,u}$ is matched filter length and Nh_u is defined as channel length. We regard $h_{l,u}^{(c)}$ as the l_{th} value of the equivalent channel tap gain, the modulated signal after filtering and channel effect are shown in Fig. 3.

At the receiver side, sample shift and frequency compensation method are used. ISI produced by adjacent symbols on both sides need to be well-balanced and assume $l_{d,u}$ samples shift after receiver filtering process.

Considering single user scenario, we merely need to consider the influence of ISI and ICI lead by CP insufficient in the i_{th} symbol.

$$R_{i|n,u} = \begin{cases} R_{i|i,n,u} + R_{i|i+1,n,u} & i = 1 \\ R_{i|i-1,n,u} + R_{i|i,n,u} + R_{i|i+1,n,u} & 0 < i < N_{sym} \\ R_{i|i-1,n,u} + R_{i|i,n,u} & i = N_{sym} \end{cases} \tag{5}$$

The $R_{i|n,u}$ is received signal of user u in the n_{th} subcarrier before FFT, which is generally compose of the current symbol $R_{i|i,n,u}$, former symbol $R_{i|i-1,n,u}$ and latter symbol $R_{i|i+1,n,u}$. N_{sym} represents symbol number.

The k_{th} sample of desired signal $R_{i|i,n,u}$ is also compose of three parts as Fig. 3 shows.

$$\begin{aligned} &R_{i|i,n,u}(k) \\ &= d_{i,n} \sum_{l=0}^{l_{d,u}-1} h_{l,u}^{(c)} e^{\frac{j2\pi n\left(k+l_{d,u}-l\right)}{N_{FFT,u}}} u(l-k-l_{d,u}+N_{FFT,u}-1) \\ &\quad + d_{i,n} \sum_{l=l_{d,u}}^{l_{d,u}+N_{cpu}} h_{l,u}^{(c)} e^{j2\pi n(k+l_{d,u}-l)/N_{FFT,u}} \\ &\quad + d_{i,n} \sum_{l=l_{d,u}+N_{cp_u}}^{Nh_u^{(c)}-1} h_{l,u}^{(c)} e^{\frac{j2\pi n\left(k+l_{d,u}-l\right)}{N_{FFT,u}}} u(k-l+l_{d,u}+N_{cp_u}) \\ &0 \le k \le N_{FFT,u}-1 \end{aligned} \tag{6}$$

Among (6), $d_{i,n}$ denotes modulated signal on the n_{th} subcarrier of the i_{th} symbol and N_{cp_u} denotes the CP length of user u. The first part and third part of (6) contain information of latter symbol and former symbol for the k_{th} sample, respectively. Then, we use unit step function $u(\cdot)$ to remove unwanted sampling information. The second part of (6) only includes current symbol information.

Then we apply FFT to symbol i . Signal on the n_{th} subcarrier is

$$\begin{aligned} &Y_{i|i,n,u} \\ &= \frac{1}{N_{FFT,u}} d_{i,n} \left[\sum_{l=0}^{l_{d,u}-1} h_{l,u}^{(c)} e^{-\frac{j2\pi nl}{N_{FFT,u}}} \left(N_{FFT,u} - l_{d,u} + l\right) \right. \\ &\quad + \sum_{l=l_{d,u}}^{l_{d,u}+N_{cpu}} h_{l,u}^{(c)} e^{-\frac{j2\pi nl}{N_{FFT,u}}} \\ &\quad \left. + \sum_{l=l_{d,u}+N_{cpu}}^{Nh_u^{(c)}-1} h_{l,u}^{(c)} e^{-\frac{j2\pi nl}{N_{FFT,u}}} \left(N_{FFT,u} + l_{d,u} - l\right) \right] \end{aligned} \tag{7}$$

it can be simplified expressed as $Y_{i|i,n,u} = d_{i,n} \times I_n$, where I_n represents the variation of symbol amplitude. Then, the average power of the desired signal on the n_{th} subcarrier is $E\left(P_{n,u}^{DES}\right) = E\left(d_{i,n}^2 I_n{}^2\right) = \sigma_{x,u}^2 I_n{}^2$. We assume the signal power of user u is $\sigma_{x,u}^2 = 1$.

B. ICI FOR CP INSUFFICIENT

The ICI component of user u received in subcarrier n is

$$\begin{aligned} &R_{i|i,m\neq n,u}^{ICI}(k) = \sum_{\substack{m=n_u \\ m\neq n}}^{N_u+n_u-1} d_{i,m} \\ &\quad \times \left[\sum_{l=0}^{l_{d,u}-1} h_{l,u}^{(c)} e^{\frac{j2\pi m\left(k+l_{d,u}-l\right)}{N_{FFT,u}}} u\left(k-l-l_{d,u}+N_{FFT,u}\right) \right. \\ &\quad \left. + \sum_{l=l_{d,u}+N_{cpu}+1}^{Nh_u^{(c)}-1} h_{l,u}^{(c)} e^{\frac{j2\pi m\left(k+l_{d,u}-l\right)}{N_{FFT,u}}} u(l-k-l_{d,u}-N_{cp_u}-1) \right] \\ &0 \le k \le N_{FFT,u}-1 \end{aligned} \tag{8}$$

The two parts in (8) are all because during the sampling of symbol i, the symbol $i+1$ and symbol $i-1$ occupy several samples among them. The orthogonality between subcarriers is destroyed and the amplitude of other subcarriers

at the sampling point of target subcarrier is no longer zero. As shown in Fig. 3, Samples in part 2 belong to the same symbol and satisfy the orthogonal condition, thus no ICI is produced here. The other 2 parts lose their orthogonality by the influence of adjacent symbols and cause ICI. After FFT operation, the ICI in subcarrier n is

$$Y^{ICI}_{i|i,m\neq n,u} = -\frac{1}{N_{FFT,u}} \sum_{\substack{m=n_u-1 \\ m\neq n}}^{N_u+n_u-1} d_{i,m} \times \left[\sum_{l=0}^{l_{d,u}-1} \sum_{k=N_{FFT,u}-l_{d,u}+l-1}^{N_{FFT,u}-1} h^{(c)}_{l,u} e^{\frac{j2\pi m\left(k+l_{d,u}-l\right)}{N_{FFT,u}}} e^{-\frac{j2\pi n\left(k+l_{d,u}\right)}{N_{FFT,u}}} + \sum_{l=l_{d,u}+N_{cpu}}^{Nh^{(c)}_u-1} \sum_{k=0}^{l-l_{d,u}-N_{cpu}} h^{(c)}_{l,u} e^{\frac{j2\pi m\left(k+l_{d,u}-l\right)}{N_{FFT,u}}} e^{-\frac{j2\pi n\left(k+l_{d,u}\right)}{N_{FFT,u}}} \right] \tag{9}$$

The negative sign in (9) shows the fact that the ICI can also be described as the gap between the ICI in practice and the desired ICI, for the reason that the desired ICI is zero. As a consequence, we only calculate the opposite value of areas with oblique line within each symbol in Fig. 3 for the sake of calculation simplicity. The ICI is further written as $Y^{ICI}_{i|i,m\neq n,u} = \sum_{\substack{m=n_u-1 \\ m\neq n}}^{N_u+n_u-1} d_{i,m} I^{ICI}_{m,n}$, where $I^{ICI}_{m,n}$ represents interference coefficient that $d_{i,m}$ caused to $d_{i,n}$. The average power of $Y^{ICI}_{i|i,m\neq n,u}$ is $E\left(P^{ICI}_{m\neq n,u}\right) = \sigma^2_{x,u} \sum_{\substack{m=n_m-1 \\ m\neq n}}^{N_m+n_m-1} \left(I^{ICI}_{m,n}\right)^2$.

C. ISI FOR CP INSUFFICIENT

The ISI is caused by the former symbol and the latter symbol. The form is similar to the previous sections, but the differences are that we are no longer considering data of the current symbol merely. The data of adjacent symbols and all subcarriers of target user should be taken into consideration simultaneously.

(10)-(11), as shown at the top of the next page, describe the ISI caused by the previous symbol to the n_{th} subcarrier and (12)-(13), as shown at the top of the next page, describe the ISI caused by the next symbol.

The two parts of ISI correspond to part 3 and part 1 in Fig. 3, respectively. (11) and (13) can be written as $Y^{ISI}_{i|i-1,n,u} = \sum_{m=n_u-1}^{N_u+n_u-1} d_{i-1,m} I^{ISI,pre}_{m,n}$ and $Y^{ISI}_{i|i+1,n,u} = \sum_{m=n_u-1}^{N_u+n_u-1} d_{i+1,m} I^{ISI,nex}_{m,n}$. And the average power of two expressions mentioned above express as $E\left(P^{ISI,pre}_{n,u}\right) = \sigma^2_{x,u} \sum_{m=n_m-1}^{N_m-1} \left(I^{ISI,pre}_{m,n}\right)^2$ and $E\left(P^{ISI,nex}_{n,u}\right) = \sigma^2_{x,u} \sum_{m=n_m-1}^{N_m-1} \left(I^{ISI,nex}_{m,n}\right)^2$ respectively.

If the target symbol is the first or the last symbol, you should only consider the ISI of the next symbol or the previous symbol, respectively. And for single user, three symbols at most need to be calculated to get the derivation of interference.

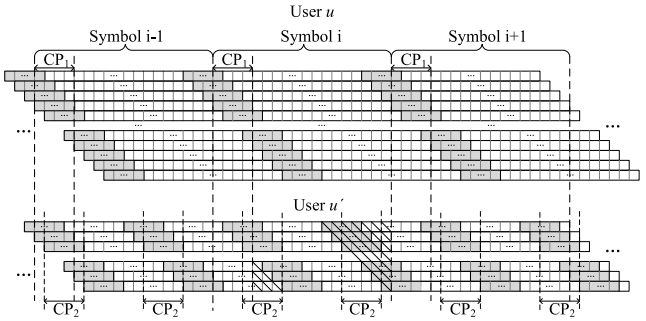

FIGURE 4. Schematic diagram of relationships between symbols of different users in multi-user scenarios.

D. INTERFERENCE FOR MULTI USER

We mainly study the IUI caused by users who have different subcarrier spacing and hence also have different symbol length. It is assumed that the interference user processes wider subcarrier spacing and shorter symbol length. Concerned with the flexible symbol length of all users, there is not a fixed correspondence between symbols of different users as Fig. 4 shows. The relationships between symbols of different users are also not fixed. Areas with oblique line are used to distinguish different symbols. If we only concern unified numerology in synchronous scenarios [22], the IUI caused by different subcarrier spacing between users as shown in Fig. 5 and Fig. 9 will almost not exist and it is not a comprehensive description for an F-OFDM system.

The corresponding symbols of interference user u' to the i_{th} symbol of target user u is expressed as

$$\begin{aligned} i_{u'}-1 \leq \frac{(i_u-1)N_{FFT_u} + k + N_{cp_u} + l_{d,u} - l^{u'} - \tau_{u'}}{N_{FFT_{u'}}} < i_{u'} \\ 0 \leq k \leq N_{FFT_u} - 1 \end{aligned} \tag{14}$$

where $i_{u'}$ and i_u are ordinal numbers of interference user symbol and target user symbol. $\tau_{u'}$ is relative delay between the two users.

We obtain the practical range of k when calculating interference introduced by $i_{u'}$, which is given by

$$\begin{aligned} k &\geq (i_{u'}-1)N_{FFT_{u'}} - (i_u-1)N_{FFT_u} \\ &\quad - \left(N_{cp_u} + l_{d,u} - l^{u'} - \tau_{u'}\right) \\ k &< i_{u'}N_{FFT_{u'}} - (i_u-1)N_{FFT_u} \\ &\quad - \left(N_{cp_u} + l_{d,u} - l^{u'} - \tau_{u'}\right) \end{aligned} \tag{15}$$

because sampling point k has a range of $\left[0, N_{FFT_u}-1\right]$, then we derive the symbol number range of interference user for

$$R^{ISI}_{i|i-1,m,u}(k)=\sum_{m=n_u-1}^{N_u+n_u-1} d_{i-1,m}\sum_{l=l_{d,u}+N_{cpu}+1}^{Nh_u^{(c)}-1} h^{(c)}_{l,u}e^{\frac{j2\pi m\left(k+l_{d,u}-l+N_{cpu}\right)}{N_{FFT,u}}}u\left(l-k-l_{d,u}-N_{cp_u}-1\right),0\le k\le N_{FFT,u}-1 \quad (10)$$

$$Y^{ISI}_{i|i-1,n,u}=\frac{1}{N_{FFT,u}}\sum_{m=n_u-1}^{N_u+n_u-1} d_{i-1,m}\sum_{l=l_{d,u}+N_{cpu}+1}^{Nh_u^{(c)}-1}\sum_{k=1}^{l-l_{d,u}-N_{cpu}-1} h^{(c)}_{l,u}e^{\frac{j2\pi m\left(N_{cpu}+k+l_{d,u}-l\right)}{N_{FFT,u}}}e^{\frac{-j2\pi n\left(k+l_{d,u}\right)}{N_{FFT,u}}} \quad (11)$$

$$R^{ISI}_{i|i+1,m,u}(k)=\sum_{m=n_u-1}^{N_u+n_u-1} d_{i+1,m}\sum_{l=0}^{l_{d,u}-1} h^{(c)}_{l,u}e^{\frac{j2\pi m\left(k+l_{d,u}-l+N_{cpu}\right)}{N_{FFT,u}}}u\left(k-l+l_{d,u}-N_{FFT,u}\right),0\le k\le N_{FFT,u}-1 \quad (12)$$

$$Y^{ISI}_{i|i+1,n,u}=\frac{1}{N_{FFT,u}}\sum_{m=n_u-1}^{N_u+n_u-1} d_{i+1,m}\sum_{l=0}^{l_{d,u}-1}\sum_{k=N_{FFT,u}-l_{d,u}+l-1}^{N_{FFT,u}-1} h^{(c)}_{l,u}e^{\frac{j2\pi m\left(k+l_{d,u}-l-N_{cpu}-N_{FFT,u}\right)}{N_{FFT,u}}}e^{\frac{-j2\pi n\left(k+l_{d,u}\right)}{N_{FFT,u}}} \quad (13)$$

$$SINR_{u,n}=\frac{E\left(P^{DES}_{n,u}\right)}{E\left(P^{ICI}_{m\neq n,u}\right)+E\left(P^{ISI,pre}_{n,u}\right)+E\left(P^{ISI,nex}_{n,u}\right)+E\left(P^{inter}_{n,u}\right)+\sigma^2_{u,Z}} \quad (20)$$

each symbol in target user from (14)and (15)

$$\begin{aligned} i_{u',\min,i_u} &\ge \frac{(i_u-1)N_{FFT_u}+N_{cp_u}+l_{d,u}-l^{u'}_{\max}-\tau_{u'}}{N_{FFT_{u'}}}+1\\ i_{u',\max,i_u} &\le \frac{(i_u-1)N_{FFT_u}+N_{cp_u}+l_{d,u}-l^{u'}_{\min}-\tau_{u'}}{N_{FFT_{u'}}} \end{aligned} \quad (16)$$

Combined effect of channel and filters for interference is $h^{(c)}_{u'}=f_{u'}*h_u*f_u^*$. The length of $h_{u'}$ is $Nh^{(c)}_{u'}=Nh_u+L_{f,u'}+L_{f^*,u'}-2$, which equals to $l^{u'}_{\max}+1$, and $l^{u'}_{\min}$ is zero. And the range of $l^{u'}$ is $\left[l^{u'}_{\min},l^{u'}_{\max}\right]$. Equivalent symbol sequence number and sampling point of interference user is

$$i_{u'}=\left\lfloor\frac{(i_u-1)N_{FFT_u}+k+N_{cp_u}+l_{d,u}-l^{u'}-\tau_{u'}}{N_{FFT_{u'}}}\right\rfloor \quad (17)$$

$$\begin{aligned} k_{u'} &= \left((i_u-1)N_{FFT_u}+k+N_{cp_u}+l_{d,u}-l^{u'}-\tau_{u'}\right)\\ &\quad-(i_{u'}-1)N_{FFT_{u'}}-N_{cp_u} \end{aligned} \quad (18)$$

$$\begin{aligned} Y_{i_u|i_{u'},n} &= \frac{1}{N_{FFT_u}}\sum_{i_{u'}=i_{u',\min,i_u}}^{i_{u',\max,i_u}}\sum_{m=n_{u'}-1}^{N_{u'}+n_{u'}-1} d_{i_{u'},m}\\ &\quad\times\sum_{l=0}^{Nh^{(c)}_{u'}-1}\sum_{k=k_{\min}}^{k_{\max}} h^{(c)}_{l,u'}e^{\frac{j2\pi mk_{u'}}{N_{FFT_{u'}}}}e^{-\frac{j2\pi n\left(k+l_{d,u}\right)}{N_{FFT_u}}} \end{aligned} \quad (19)$$

The bound of k references to (15) and the total interference to the symbol i_u described in (19) can be further written as $Y_{i_u|i_{u'},n}=\sum_{i_{u'}=i_{u',\min,i_u}}^{i_{u',\max,i_u}}\sum_{m=n_{u'}-1}^{N_{u'}+n_{u'}-1} d_{i_{u'},m}I^{u'}_{m,n}$. The average power of multi user interference in symbol i_{target} is $E\left(P^{u'}_{n,u}\right)=\sigma^2_{x,u'}\left(\sum_{i_{u'}=i_{u',\min,i_u}}^{i_{u',\max,i_u}}\sum_{m=n_{u'}-1}^{N_{u'}+n_{u'}-1}\left(I^{u'}_{m,n,i_{u'}}\right)^2\right)$, which demonstrates that the result is related to symbol sequence number and varies with the numerology of both users we concerned. When the users take the same numerology into consideration, the result will be similar to [22]. When interference is too large between users, bigger guard band is needed to obtain larger out-of-band attenuation.

The analysis of OFDM also like that of F-OFDM, the only difference is it does not apply filter, hence $h^c_u=h_u$ here, and the numerologies are all the same between users. Therefore, unnecessary details will not be repeated here.

E. BER ANALYSIS AND SPECTRUM EFFICIENCY

SINR on the n_{th} subcarrier of the target user is derived as (20) and $\sigma^2_{u,Z}$ is variance of AWGN in frequency domain. We employ high-order square QAM modulation scheme, and transmitted signal power is normalized $\sigma^2_{x,u}=1$.

The capacity of the target user on the n_{th} subcarrier is given as $C_{u,n}=\Delta f_u\log_2\left(1+SINR_{u,n}\right)$.

Reference to [37], [40], we compute BER in (21) of user u in sub-carrier n according to SINR in (20), as shown at the top of this page.

$$\begin{aligned} P_{e,u,n} &\cong \frac{\sqrt{M}-1}{\sqrt{M}\log_2\left(\sqrt{M}\right)}erfc\left(\sqrt{\frac{3\log_2(M)}{2(M-1)}SINR_{u,n}}\right)\\ &\quad+\frac{\sqrt{M}-2}{\sqrt{M}\log_2\left(\sqrt{M}\right)}erfc\left(3\sqrt{\frac{3\log_2(M)}{2(M-1)}SINR_{u,n}}\right) \end{aligned} \quad (21)$$

In high SINR, the first term in (21) is dominant and is enough for analysis, but in lower SINR, if the second term omitted, the theoretical curves will deviate from the measure curves. Higher order terms are neglected because they have little effect on the results while increasing calculation difficulty. The average BER of target user is expressed as $P_{e,u} = \sum_{n=n_u-1}^{N_u+n_u-1} P_{e,u,n}/N_u$.

IV. MODEL ANALYSIS AND PROBLEM SOLVING

A. MODEL ANALYSIS

The proposed optimization problem does not have a directly solving method because of the existence of ISI, ICI and IUI. We take ISI for example. ICI and IUI have similar analysis method.

The simplest case is to consider interference only from one symbol in single subcarrier which is also without loss of generality. Then the ISI is represented as

$$Y^{ISI}_{i|i+1,n,u} = \frac{d_{i+1,n}}{N_{FFT,u}} \sum_{l=0}^{l_{d,u}-1} h^{(c)}_{l,u}(l_{d,u}-l) e^{\frac{j2\pi n\left(-N_{cp_u}-l\right)}{N_{FFT,u}}} \tag{22}$$

where

$$h^{(c)}_{l,u} = \sum_{j=0}^{Nh_u-1} \left(\sum_{i=0}^{L_{f,u}-1} f_u(i) f_u{}^*(j-i) \right) h_u(l-j) \tag{23}$$

According to (23), each item in the $h^{(c)}_{l,u}$ is a function of α, and the arbitrary item in $h^{(c)}_{l,u}$ is represented as the form of $h^{(c)}_{l,u}(n) = f_u(n_1) f_u{}^*(n_2) h_u(n_3)$, where n_1, n_2, n_3 is arbitrary combination that meets the requirements of (23).

The amplitude and phase of $h^{(c)}_{l,u}$ are expressed as $A^{(c)}_{l,u}$ and $\theta^{(c)}_{l,u}$. The ISI is rewritten as (24) and the power of ISI is described in (25).

$$Y^{ISI}_{i|i+1,n,u} = \frac{d_{i+1,n}}{N_{FFT,u}} \sum_{l=0}^{l_{d,u}-1} A^{(c)}_{l,u}(l_{d,u}-l) e^{j\left(\theta^{(c)}_{l,u} - \frac{2\pi n\left(N_{cp_u}+l\right)}{N_{FFT,u}}\right)} \tag{24}$$

$$P^{ISI,nex}_{n,u} = \frac{\left(\sum_{l=0}^{l_{d,u}-1} A^{(c)}_{l,u}(l_{d,u}-l) e^{\left(j\theta^{(c)}_{l,u} - \frac{j2\pi n\left(N_{cp_u}+l\right)}{N_{FFT,u}}\right)} \right)^2}{{N_{FFT,u}}^2} \tag{25}$$

where $f(\alpha)$ represents numerator of (25), and $\Theta^{(c)}_{l,u} = 2\pi n(-N_{cp_u}-l)/N_{FFT,u} + \theta^{(c)}_{l,u}$ for convenience. According to product to sum formula, the properties of function (23) is obtained in (26).

$$f'(\alpha) = 2 \left(\sum_{i=1}^{l_{d,u}-1} \sum_{j=1}^{l_{d,u}-1} A^{(c)}_{i,u} \left(A^{(c)}_{j,u}\right)' \cos(\Theta^{(c)}_{i,u} - \Theta^{(c)}_{j,u}) \right) \tag{26}$$

When we do not consider the impact of multi-path fading channel, phase variation does not exist. $\theta^{(c)}_{l,u} = 0$ and $\Theta^{(c)}_{l,u} = 2\pi n(-N_{cp_u}-l)/N_{FFT,u}$ in this case. Then $h^{(c)}_{l,u}(n)$ is rewritten as

$$h^{(c)}_{l,u}(n) = k(n) * \frac{J_0(a\alpha)}{J_0(\alpha)} * \frac{J_0(b\alpha)}{J_0(\alpha)} \quad 0 \le a,b < 1 \tag{27}$$

where $k(n)$ is the corresponding positive constant. To prove the changing trend of $h^{(c)}_{l,u}$ with α, $k(n)$ has no effect on the results and the derivative of variable part in (27) is shown as

$$\begin{aligned} g_1(\alpha) = {} & \frac{1}{{J_0}^3(\alpha)} (aJ_1(a\alpha)J_0(b\alpha)J_0(\alpha) \\ & + bJ_1(b\alpha)J_0(a\alpha)J_0(\alpha) \\ & - 2J_0(a\alpha)J_0(b\alpha)J_1(\alpha)) \quad 0 \le a,b < 1 \end{aligned} \tag{28}$$

where $J_0(\alpha)$ is zero-order modified Bessel function and is always positive when $\alpha > 0$. Contents in bracket of (28) are further written as

$$\begin{aligned} g_2(\alpha) = {} & (aJ_1(a\alpha)J_0(\alpha) - J_0(a\alpha)J_1(\alpha)) J_0(b\alpha) \\ & + (bJ_1(b\alpha)J_0(\alpha) - J_0(b\alpha)J_1(\alpha)) J_0(a\alpha) \\ & 0 \le a, b < 1 \end{aligned} \tag{29}$$

where $J_0(a\alpha)$ and $J_0(b\alpha)$ are positive, the two terms of (29) have similar representation and properties. Further calculation is shown in (30).

$$\begin{aligned} & g_3(\alpha) \\ & = aJ_1(a\alpha)J_0(\alpha) - J_0(a\alpha)J_1(\alpha) \\ & = a\left(1+\sum_{k=1}^{\infty} \frac{\alpha^{2k}}{\left(k!2^k\right)^2}\right)\left(a^{2k}\sum_{k=1}^{\infty} 2k\frac{\alpha^{2k-1}}{\left(k!2^k\right)^2}\right) \\ & \quad -\left(1+\sum_{k=1}^{\infty} \frac{(a\alpha)^{2k}}{\left(k!2^k\right)^2}\right)\left(\sum_{k=1}^{\infty} 2k\frac{\alpha^{2k-1}}{\left(k!2^k\right)^2}\right) \\ & = \left(a^{2k+1}-1\right)\left(\sum_{k=1}^{\infty} 2k\frac{\alpha^{2k-1}}{\left(k!2^k\right)^2}\right) \\ & \quad + a^{2k}(a-1)\left(\sum_{k=1}^{\infty} \frac{\alpha^{2k}}{\left(k!2^k\right)^2}\right)\left(\sum_{k=1}^{\infty} 2k\frac{\alpha^{2k-1}}{\left(k!2^k\right)^2}\right) \end{aligned} \tag{30}$$

where $0 \le a < 1$, $\left(a^{2k+1}-1\right)$ and $(a-1)$ are all negative, thus $g_3(\alpha)$ is negative. $g_2(\alpha)$ is negative as well. $g_1(\alpha)$ and $A^{(c)}_{l,u}$ decrease monotonously with the increase of α. In (26), $A^{(c)}_{i,u} > 0$, $\left(A^{(c)}_{j,u}\right)' < 0$, the value of $\cos(\Theta^{(c)}_{i,u} - \Theta^{(c)}_{j,u})$ cannot be directly determined because it is periodic and the value changes with the subcarrier index n .

When considering the impact of multi-path fading channel, phase $\theta^{(c)}_{l,u}$ is not zero anymore, it changes with the phase of channel. And we cannot get $f'(\alpha)$. Reference to Fig. 7(a), we also observe that $f(\alpha)$ is neither monotonous nor a function with convexity and concavity.

ISI is nonconvex and nonmonotonic. ISI, ICI and IUI have same properties. SINR in (20) is not a monotonic function, and the capacity of single subcarrier is non-concave. Similarly, the total capacity of the system is non-concave. Then the spectrum efficiency is also non-concave when the guard bandwidth and filter length are fixed. The formulated

problem is NP-hard when taking different guard bandwidth and filter length into consideration. So we would better use heuristic algorithm for the solutions.

Algorithm 1 Filter Parameters and Guard Bandwidth Optimization

1:**Input**: Number of subcarriers, subcarrier spacing and channel gain of each user
2:**Output**: Optimal spectral efficiency
3:**set**: s=0, iteration number is S,empire number is N_{imp} and total country number N
4:**calculate**: $cost_i^{(0)}$, $power_i^{(0)}$ and $N_{imp,i}^{(0)}$ for $i \in N$
5:**while** $s < S \& N_{imp} > 1$ **do**
6: $s = s + 1$
7: **update** colonies positions
8: **if**: $p_e > P_{e,target}$, **then**
9: $cost_i^{(s)} \leftarrow \infty$ for $i \in N$
10: **end if**
11: **update** $cost_i^{(s)}$ for $i \in N$ and $Tcost_i^{(s)}$ for $i \in N_{imp}$
12: **calculate** p_i for $i \in N_{imp}$
13: Empire i occupies colonies in probability p_i
14: Return step 5
15:**end while**
16:**calculate** $C^{E*} = \frac{1}{\max_i \left\{cost_i^{(s)}\right\}}$

B. IMPERIALIST COMPETITION ALGORITHM

The ICA is a swarm intelligence optimization algorithm proposed in recent years. It has faster searching speed and higher accuracy compared with other algorithms like PSO or GA [41]. The ICA mainly consist four parts, including initialization, assimilation, imperialist competition and collapse of weak empires [42]. The steps to solve the problem formulated above is shown in Algorithm1 .

The ICA initializes $N_{country}$ arrays of variable values as initialized counties. One of the countries is defined as $country = [L_1, \alpha_1, L_2, \alpha_2, \cdots, L_n, \alpha_n, B_{g,1}, \cdots, B_{g,n-1}]$ for (4). The cost of the i_{th} countries is reciprocal of spectrum efficiency and expressed as $cost_i = \frac{1}{C^E(country_i)}$. We rank the cost in ascending order and the first N_{imp} are imperialists, the other N_{col} are colonies. In order to distribute colonies to imperialists, we calculate the normalized power of i_{th} imperialist expressed as $power_i$. The number of colonies belongs to the i_{th} imperialist is $N_{imp,i} = round\ (power_i \cdot N_{col})$.

During assimilation processes, the colonies move toward imperialists with angle θ and distance D. $\theta \sim U(-\gamma, \gamma)$ with γ usually equals to $\frac{\pi}{4}$ and $D \sim U(0, d \cdot \beta)$ with β usually equals to 2, and d is the distance between the colony and its corresponding imperialist. The position of original imperialist will be replaced by colony once the cost of colony less than that of imperialist. The total cost of the i_{th} empire is represented as $Tcost_i$.

TABLE 1. Simulation Parameters.

Parameter	Value
Sampling rate	30.72 MHz
Subcarrier spacing	15 KHz/30 KHz
FFT size	2048/1024
F-OFDM CP length	160
OFDM CP length	160
Modulation mode	QAM
Modulation order	64
Sub-band filter	Kaiser Window FIR filter
Channel	Extended Pedestrian A model

In imperialist competition, the weakest colony of the weakest empire will be scrambled by other empires, with the probability p_i.

During the algorithm execution, collapse of weak empires is unavoidable and the more powerful empire occupies more colonies. However, it is important to note that if the country does not satisfy the constraints of BER, the cost of it will be set to a large value to reduce its competitiveness. The algorithm stops when the minimum cost converges.

The computational complexity of initialization is $O\left(N_{country} \times N_u^2\right)$, the complexity of producing empires is $O\left(N_{imp}\right)$, The assimilation, update and competition processes are all have computational complexity of $O\left(N_{country}\right)$. The complexities of producing empires, the assimilation, update and competition processes have similar order, then they can be combined. Because N_{imp} is smaller than $N_{country}$, then the worst case complexity of the algorithm is $O\left(N_{country} \times N_u^2\right) + O\left(N_{country}\right)$ in each iteration. The complexities of PSO and GA to solve the proposed filter parameters and guard bandwidth optimization problem are all $O\left(N \times N_u^2\right) + O\left(N\right)$ in one iteration, where N is the number of particles in PSO and the number of chromosomes in GA. N equals to $N_{country}$ and thus the ICA has same complexity with these traditional heuristic algorithms from this point. However, it has been shown in Fig. 11(c) that the ICA has fast convergence rate and needs less iterations. Therefore, the ICA is more suitable for our proposed model.

V. SIMULATION RESULTS

In the simulations, multi user situation is discussed with different numerologies in order to highlight the flexibility of the F-OFDM. The number of users is flexible in multi user scenario, and when we focus on the filter performance, users can be configured with different number of subcarriers. The simulation parameters are shown in Table 1. The sampling rate of the system is 30.72 MHz, and users with different subcarrier spacing are allocated with distinct FFT size. The CP length is initialized to 7% of symbol length to maintain consistency with OFDM, which is convenient for performance comparison.

We use Monte-Carlo simulation method to verify that the theoretical derivation of SINR fits perfectly with experimental results. The following parameters are employed

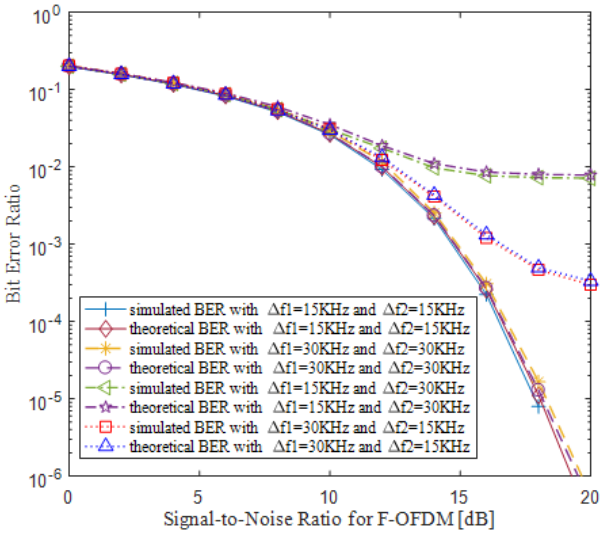

FIGURE 5. Simulated results and theoretical derivation BER performance in two users scenario with different subcarrier spacing ($\Delta f1$ for target user and $\Delta f2$ for interference one).

in the process of research: QAM modulation is adopted to increase the transmission rate. We use Kaiser Window to construct FIR filter, in which roll-off parameter and filter length is configured dynamically. Transmit filter and receive filter are same for simplification. Multi-path channel fading is characterized by Rayleigh distribution.

A. ACCURACY OF THEORETICAL DERIVATION

We verify the accuracy of theoretical derivation in this part. BER of F-OFDM and OFDM are present to prove that theoretical SINR reflects simulation results correctly which lay a solid foundation for following research.

The impact of interference between users is shown in Fig. 5. In the simulation, we take two users for example. The filter length is $L_f = 0.2 \times N$ and roll-off is $\alpha = 5$. N is the length of the symbol. The guard bandwidth is fixed to 15 KHz in order to ensure the convenience of comparison. Performances of users with 15 KHZ subcarrier spacing in two systems are compared. Then, 15 KHZ and 30 KHZ are distributed to different users. The results inferred that users with same numerology introduces less interference to others, while multi-user interference increases when utilize distinct numerologies for lack of orthogonality. What is more, users with wider subcarrier space have greater impact on users with narrower subcarrier space. That is to say, although F-OFDM possesses flexible numerologies, a dynamic filter parameters optimization scheme is still desperately needed to achieve an acceptable level of multi-user interference.

Fig. 6 illustrates the effect of time offset between users. Two users are also sufficient to reflect asynchronicity of communication links and same numerology between users is set, time delay between users of asynchronous transmission is τ. Filter length $L_f = 0.2 \times N$ and roll-off is $\alpha = 5$ in F-OFDM. It can be observed in Fig. 6(a) that with the help of sub-band filter, F-OFDM with 30 KHz guard

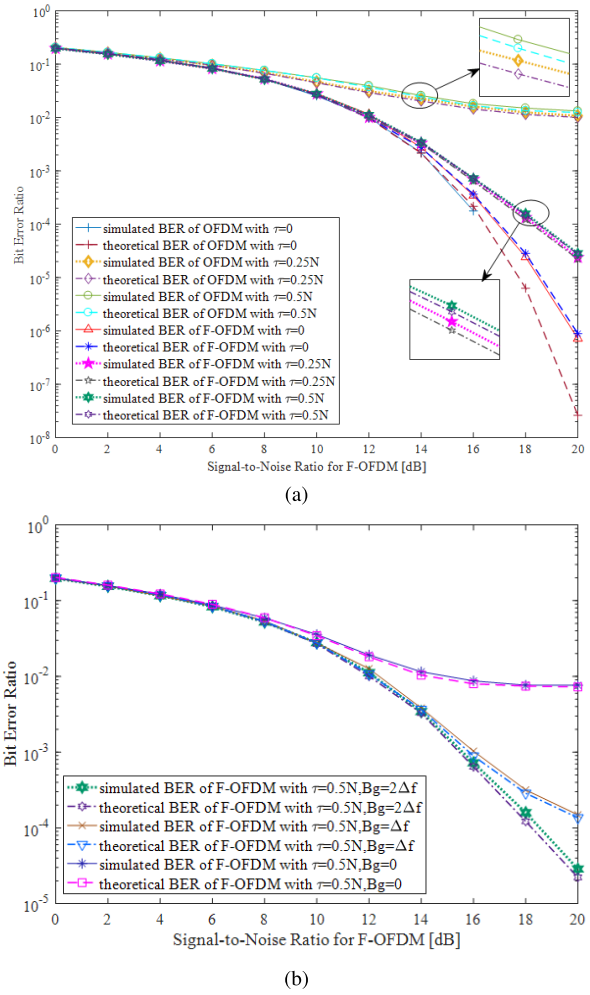

FIGURE 6. Simulated results and theoretical derivation BER performance of OFDM and F-OFDM system with different time delay τ and guard bandwidth B_g in two-user scenario.

bandwidth have stronger robustness against misalignment in time domain than that in OFDM, however, it also introduce ISI and ICI caused by filter tail. Furthermore, the BER performance difference between $0.25N$ and $0.5N$ offsets is negligible. Fig. 6(b) shows that asynchronous interference reduces effectively at the cost of wider the guard bandwidth.

Because the theoretical derivation and practical simulation are well matched, the SINR we deduced can be used in following analysis directly, and the comparison between analytical and Monte Carlo simulated results will not be presented below.

B. EFFECT OF FILTER PARAMETERS AND VARIOUS NUMEROLOGIES IN THE F-OFDM SYSTEM

Filter parameters, CP length, subcarrier spacing and guard bandwidth are investigated in this part to show the effect on F-OFDM system, in which multi user scenario is considered for a comprehensive analysis results. To make the simulation clear, we set up two users and each contains 24 subcarriers. The subcarrier spacing of the two users are 15 KHz and 30 KHz, respectively.

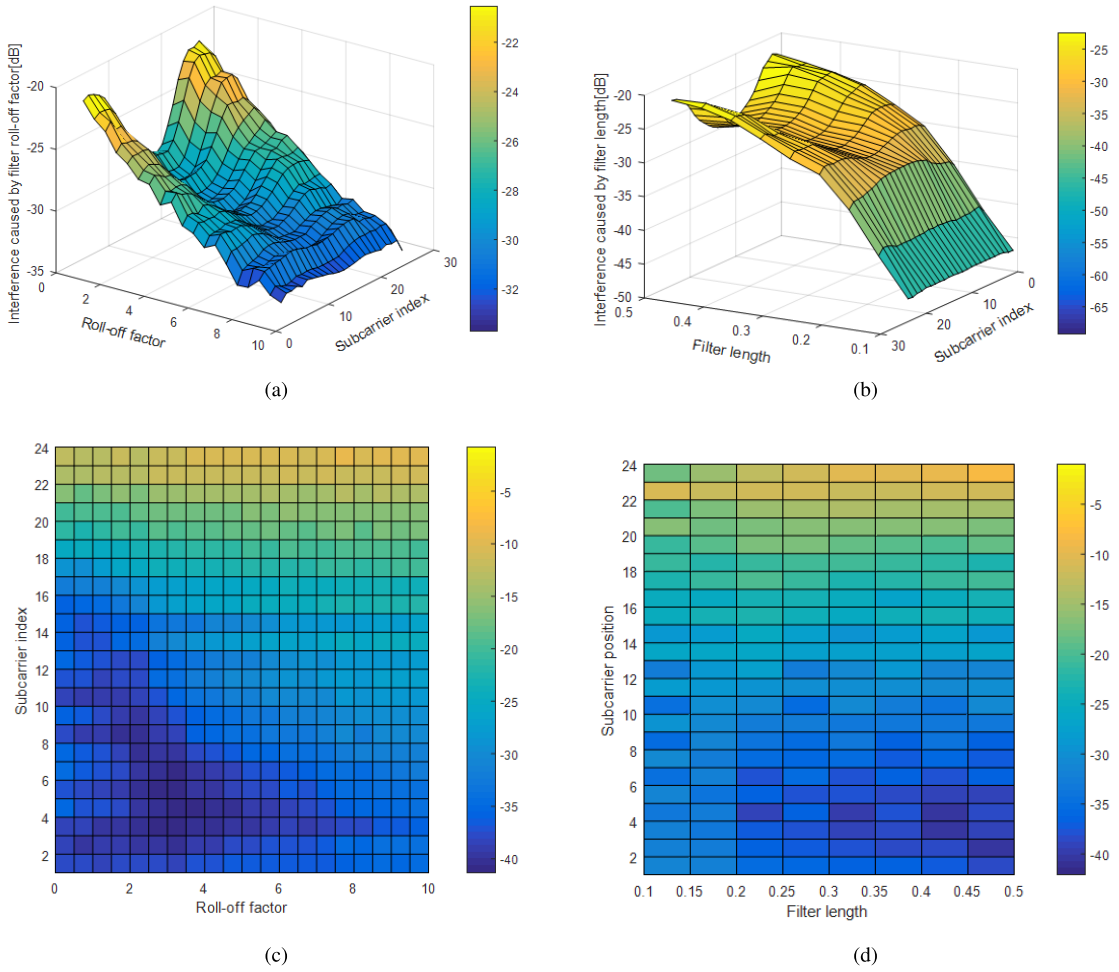

FIGURE 7. (a) Interference in each subcarrier versus different filter roll-off factor of user itself. (b) Interference in each subcarrier versus different filter length of user itself. (c) Interference in each subcarrier versus different filter roll-off factor of neighbor user. (d) Interference in each subcarrier versus different filter length of neighbor user.

We show the influence of filter roll-off and filter length on the F-OFDM system on assumption that the CP length is constant at $L_{CP} = 0.07 \times N$, α ranges from 0 to 10 and $L_f \in [0, 0.5 \times N]$. Only one value of the upper two variables is changed at a time in the simulations. User with 15 KHz subcarrier spacing is target user and the other is interference one.

Fig. 7(a)(b) show the effect of α and L on the interference of user itself, and the 3-dimensional graphs reflect the trend of interference in each subcarrier with the variation of the two coefficients. In these simulations, when the research object is α, filter length is set to be $L_f = 0.3 \times N$ which is longer than CP length in order to highlight the interference that α caused to the user itself. And when L_f turns to be a target, filter roll-off is set to $\alpha = 5$ without loss of generality. The results demonstrate that higher α value and shorter L introduce less interference under the circumstances of CP insufficient. The IUI with different α and L is also illustrated in Fig. 7(c)(d). Two-user configuration has enough representativeness for IUI analysis and two sub-bands use different subcarrier spacing magnify the variation of results we observed. The guard band between users is set to zero for sake of comparison convenient. Simulation results indicate the tendency that more multi-user interference appears with α increases which is opposite to that in Fig. 7(a) and the influence of L on the interference is hard to analyze. The IUI is change irregularly with α or L because the orthogonality of symbols in time domain is destroyed. It is clear from the upper results that both α and L need a compromise between target user performance and IUI, and it is of vital importance to choose an appropriate value.

CP is flexible in F-OFDM system, in this simulation, filter parameters are fixed to $L_f = 0.2 \times N$ and $\alpha = 2$. The relationship between CP length and interference including ISI and ICI are shown in Fig. 8. The results show that the interference is sensitive to the change of CP length. The interference drastically decreases with CP length grow and then disappears at a certain length, besides, it maintains zero after this point because CP is sufficient and interference from adjacent symbols is avoided. However, purely depend on

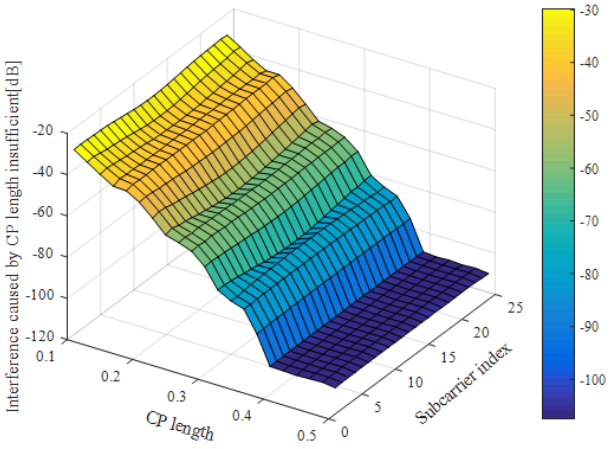

FIGURE 8. Interference in each subcarrier versus different CP length.

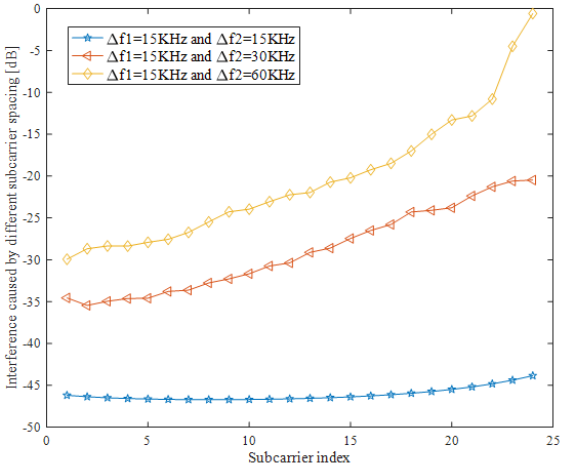

FIGURE 9. Interference power versus subcarrier index with different subcarrier spacing gap.

overlong L to pursue interference free is infeasible because CP is used for protection, if it occupies too much time resource for useful signal may lead to inefficiency of spectrum. The CP length will remain unchanged in this paper for simplification.

Subcarrier spacing is another important factor affecting the BER performance of multi-user F-OFDM system. In order to weaken the influence of the filter on the users own interference and highlight the interference among the users, we set $L_f = 0.1 \times N$ and $\alpha = 5$. It is verified from the simulation results in Fig. 9 that the interference introduced by the same subcarrier spacing is smaller than that from different subcarrier spacing. And we notice that the BER performance of users become worse as the gap between subcarriers increase which could refer to Fig. 5. The reason is that waveforms in frequency domain are not orthogonal and different symbol periods in time domain destroy the orthogonality among users. According to the results, it is easy to get a conclusion that the users with wider subcarrier space which create more

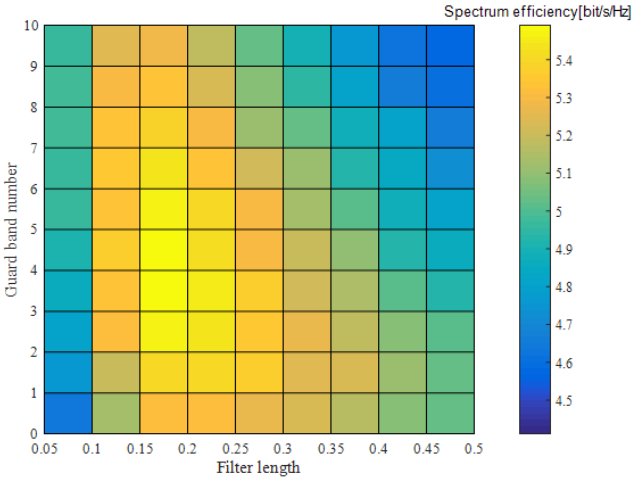

FIGURE 10. Spectrum efficiency versus different guard bandwidth and different CP length.

serious interference to other users deserve more effective filtering operation.

It is also essential to evaluate the effect of different guard bandwidth in such circumstances. SINR will be improved by enlarging the protection spacing, However, the null subcarrier, on which no data is transferred, is increased at the same time. All these indicate that the spectrum efficiency will not increase all the time just as Fig. 10 shows. $\alpha = 5$ is chosen and L_f changes in the range of $[0.05 - 0.5]$. (α changes when L_f is fixed will produce similar results and will not simulate here). For the same filter parameters, the spectrum efficiency ascends and then descends with the increase of guard bandwidth. And for the same guard bandwidth, if the filter length is insufficient, the serious IUI will be introduced, and when the filter length is too long, ISI and ICI will also occur. Therefore, it is important to optimize the filter parameters and guard bandwidth at the same time.

C. PERFORMANCE OF THE PROPOSED FILTER PARAMETERS AND GUARD BANDWIDTH OPTIMIZATION MODEL

We check the effectiveness of the proposed model and users can be configured either asynchronously or synchronously. For ICA, we set $N_{country} = 30$, $N_{imp} = 6$, $\gamma = \pi/4$ and $\beta = 2$. Iteration number is 50 and 1/4 symbol offset is maintained between users in asynchronous scenario in the simulation. Fig. 11(a)(b) shows that the spectrum efficiency of F-OFDM improves significantly after optimization for both scenarios. And from Fig. 11(c), we notice that the ICA has the fastest convergence rate when compared with PSO and GA.

In current 3GPP specification Release 15, the subcarrier spacing for OFDM is defined as $\Delta f = 15 \times 2^n, n = 0, 1, 2, \cdots$. In order to compare the capacity between the two waveforms, two 15 KHz users and two 30 KHz users are taken for example. The F-OFDM with fixed parameters [14]

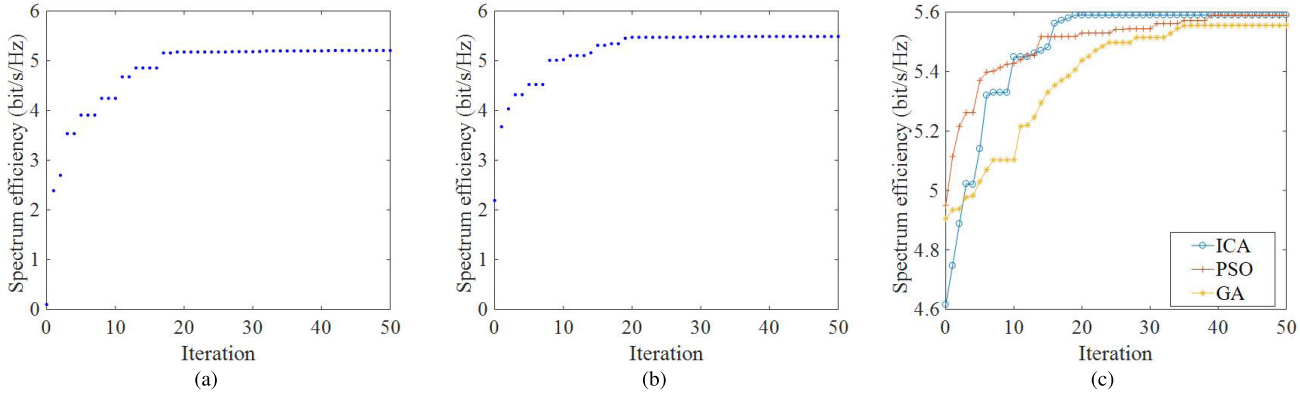

FIGURE 11. (a) Spectrum efficiency versus iterations in F-OFDM uplink asynchronous system. (b) Spectrum efficiency versus iterations in F-OFDM uplink synchronous system. (c)The comparison of convergence rate between the ICA and other algorithms.

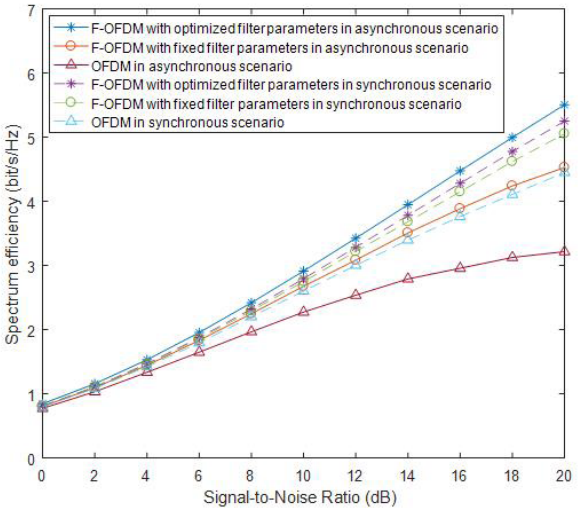

FIGURE 12. Spectrum efficiency versus SINR for different waveforms and filter parameters configurations.

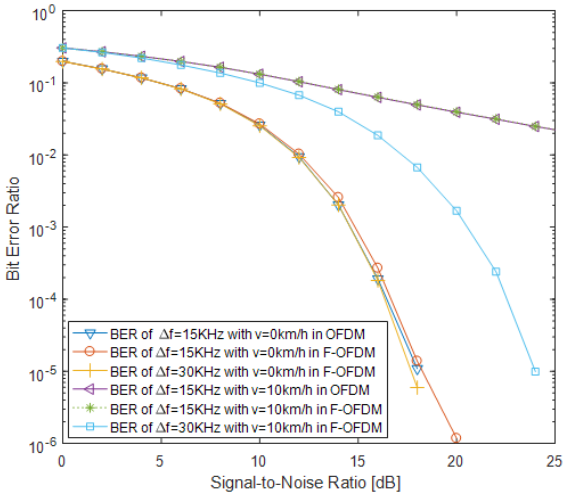

FIGURE 13. BER comparison between different subcarrier spacing with different mobile speed.

employs Hann Windowed-Sinc filters and the filter length equals to half of the symbol length. With the optimized filter parameters and guard bandwidth, the spectrum efficiency of F-OFDM outperforms OFDM and F-OFDM with optimized filter parameters is better than F-OFDM with fixed parameters as Fig. 12 shows.

D. THE EFFECT OF MOBILITY ON F-OFDM

Fig. 13 is F-OFDM and OFDM system with different mobile speed. It is clear that Doppler spread will be enhanced with the increased mobility and BER performance become worse obviously. When the two systems adopt same subcarrier spacing, no significant difference between them was noted, however, when wider subcarrier spacing is employed, the BER performance promotes greatly. This is because same mobile speed with larger subcarrier spacing corresponds to smaller Doppler spread. From this point of view, F-OFDM also has stronger ability against Doppler spread.

E. COMPARISONS BETWEEN DIFFERENT WAVEFORMS

The comparison of the power spectrum density (PSD) and BER performance between sub-band filtering waveforms are shown in Fig 14(a) and (b), respectively. F-OFDM, UFMC, W-OFDM as well as traditional OFDM are considered. There is 1/4 symbol offset between adjacent band users to highlight the asynchronous transmission performance. We clearly observe in Fig. 14(a) that OOBE performance of F-OFDM is superior to UFMC and W-OFDM because F-OFDM uses longer filter which is at the cost of introducing extra ISI and ICI. And the above mentioned waveforms for 5G all provide a better frequency-localization compared with the traditional OFDM. Besides, the F-OFDM has best BER performance over the others which are shown in Fig. 14(b). Moreover, because the proposed model achieves a balance between intra-user interference and inter-user interference, the optimized F-OFDM has the lowest BER although its out-of-band suppression is slightly worse than the conventional F-OFDM [14].

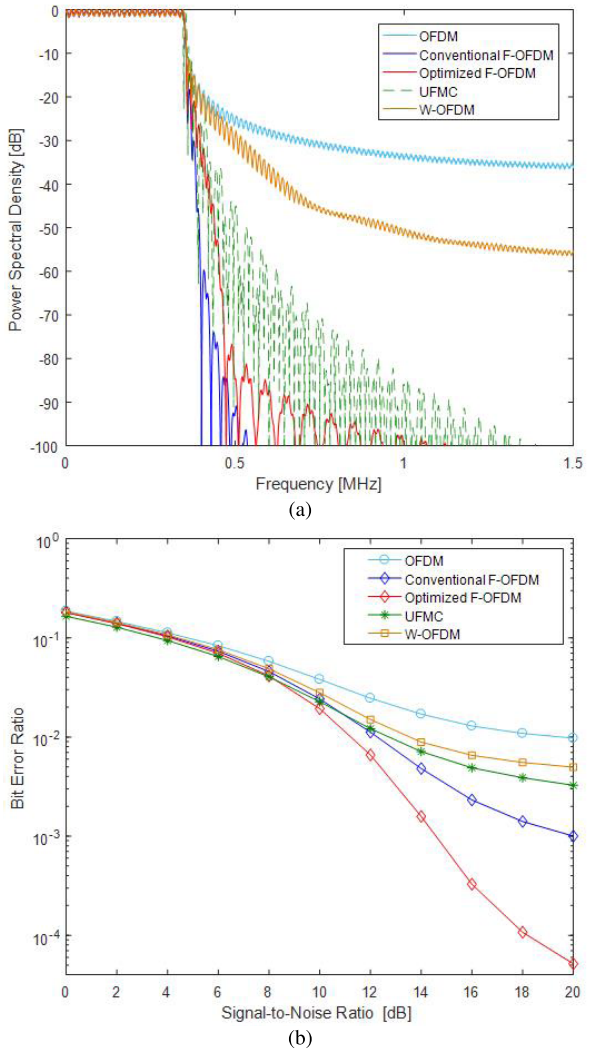

FIGURE 14. **(a)PSD comparisons for different waveforms. (b) BER comparisons for different waveforms.**

VI. CONCLUSION

In this paper, we have derived interference and BER in multi user F-OFDM system with a variety of numerologies theoretically and the derivations are valid. Important factors like filter parameters, CP length, subcarrier spacing, guard bandwidth and the degree of asynchronization largely affect the performance of F-OFDM. We proposed a filter parameters and guard bandwidth optimization model to configure parameters suitably and to get maximized spectral efficiency based on the theoretical analysis for asynchronous uplink F-OFDM system. Optimization parameters are achieved with the help of ICA. Simulation results show that the proposed model in F-OFDM can balance IUI and interference from users themselves effectively and help the system obtain optimized spectrum efficiency. Besides, F-OFDM outperforms conventional OFDM in many aspects such as in against Doppler spread and asynchronous. F-OFDM with optimized filter parameters achieves more capacity than F-OFDM with fixed filter parameters. However, the effect of Doppler spread is weakened by widening the subcarrier spacing, which reduces ICI at the expense of introducing IUI. And the balance between ICI and IUI needs further researched in the future work.

REFERENCES

[1] J. Krause, *Study on Scenarios and Requirements for Next Generation Access Technology*, document 3GPP TR 38.913, Jun. 2018.

[2] M. Series, *IMT Vision-Framework and overall objectives of the future development of IMT for 2020 and beyond*, document Rec. ITU-R M.2083-0, 2015.

[3] L. Dong *et al.*, "Introduction on IMT-2020 5G trials in China," *IEEE J. Sel. Areas Commun.*, vol. 35, no. 8, pp. 1849–1866, Aug. 2017.

[4] J. Wang *et al.*, "Spectral efficiency improvement with 5G technologies: Results from field tests," *IEEE J. Sel. Areas Commun.*, vol. 35, no. 8, pp. 1867–1875, Aug. 2017.

[5] X. Zhang, L. Chen, J. Qiu, and J. Abdoli, "On the waveform for 5G," *IEEE Commun. Mag.*, vol. 54, no. 11, pp. 74–80, Nov. 2016.

[6] B. Farhang-Boroujeny and H. Moradi, "OFDM inspired waveforms for 5G," *IEEE Commun. Surveys Tuts.*, vol. 18, no. 4, pp. 2474–2492, 4th Quart., 2016.

[7] Y. Cai, Z. Qin, F. Cui, G. Y. Li, and J. A. McCann, "Modulation and multiple access for 5G networks," *IEEE Commun. Surveys Tuts.*, vol. 20, no. 1, pp. 629–646, 1st Quart., 2018.

[8] D. Zhang, M. Matthé, L. L. Mendes, and G. Fettweis, "A study on the link level performance of advanced multicarrier waveforms under MIMO wireless communication channels," *IEEE Trans. Wireless Commun.*, vol. 16, no. 4, pp. 2350–2365, Apr. 2017.

[9] M. Bellanger *et al.*, "FBMC physical layer: A primer," *PHYDYAS*, vol. 25, no. 4, pp. 7–10, Jan. 2010.

[10] N. Michailow *et al.*, "Generalized frequency division multiplexing for 5th generation cellular networks," *IEEE Trans. Commun.*, vol. 62, no. 9, pp. 3045–3061, Sep. 2014.

[11] X. Chen, L. Wu, Z. Zhang, J. Dang, and J. Wang, "Adaptive modulation and filter configuration in universal filtered multi-carrier systems," *IEEE Trans. Wireless Commun.*, vol. 17, no. 3, pp. 1869–1881, Mar. 2018.

[12] *Link.level Evaluation of Filtered/Windowed OFDM*, Intel Corporation, Nanjing, China, May 2016.

[13] J. Abdoli, M. Jia, and J. Ma, "Filtered OFDM: A new waveform for future wireless systems," in *Proc. IEEE 16th Int. Workshop Signal Process. Adv. Wireless Commun. (SPAWC)*, Jun./Jul. 2015, pp. 66–70.

[14] X. Zhang, M. Jia, L. Chen, J. Ma, and J. Qiu, "Filtered-OFDM—Enabler for flexible waveform in the 5th generation cellular networks," in *Proc. IEEE Global Commun. Conf. (GLOBECOM)*, Dec. 2015, pp. 1–6.

[15] J. Nadal, C. A. Nour, and A. Baghdadi, "Design and evaluation of a novel short prototype filter for FBMC/OQAM modulation," *IEEE Access*, vol. 6, pp. 19610–19625, 2018.

[16] D. Qu, F. Wang, Y. Wang, T. Jiang, and B. Farhang-Boroujen, "Improving spectral efficiency of FBMC-OQAM through virtual symbols," *IEEE Trans. Wireless Commun.*, vol. 16, no. 7, pp. 4204–4215, Jul. 2017.

[17] Y. Tian, D. Chen, K. Luo, and T. Jiang, "Prototype filter design to minimize stopband energy with constraint on channel estimation performance for OQAM/FBMC systems," *IEEE Trans. Broadcast.*, to be published.

[18] R. Gerzaguet *et al.*, "The 5G candidate waveform race: A comparison of complexity and performance," *EURASIP J. Wireless Commun. Netw.*, vol. 2017, no. 1, p. 13, 2017.

[19] M. Towliat and S. M. J. A. Tabatabaee, "GFDM interference mitigation without noise enhancement," *IEEE Commun. Lett.*, vol. 22, no. 5, pp. 1042–1045, May 2018.

[20] L. Zhang, A. Ijaz, P. Xiao, and R. Tafazolli, "Multi-service system: An enabler of flexible 5G air interface," *IEEE Commun. Mag.*, vol. 55, no. 10, pp. 152–159, Oct. 2017.

[21] A. Farhang, N. Marchetti, and L. E. Doyle, "Low-complexity modem design for GFDM," *IEEE Trans. Signal Process.*, vol. 64, no. 6, pp. 1507–1518, Mar. 2016.

[22] S. Wang, J. S. Thompson, and P. M. Grant, "Closed-form expressions for ICI/ISI in filtered OFDM systems for asynchronous 5G uplink," *IEEE Trans. Commun.*, vol. 65, no. 11, pp. 4886–4898, Nov. 2017.

[23] D. Wu *et al.*, "A field trial of f-OFDM toward 5G," in *Proc. IEEE Globecom Workshops (GC Wkshps)*, Dec. 2016, pp. 1–6.

[24] J. Wang *et al.*, "Field trials on spectral efficiency improvement in massive MIMO systems," in *Proc. IEEE 87th Veh. Technol. Conf. (VTC Spring)*, Jun. 2018, pp. 1–5.
[25] T. Wang, J. G. Proakis, E. Masry, and J. R. Zeidler, "Performance degradation of OFDM systems due to Doppler spreading," *IEEE Trans. Wireless Commun.*, vol. 5, no. 6, pp. 1422–1432, Jun. 2006.
[26] P. Guan *et al.*, "5G field trials: OFDM-based waveforms and mixed numerologies," *IEEE J. Sel. Areas Commun.*, vol. 35, no. 6, pp. 1234–1243, Jun. 2017.
[27] M. Iwabuchi *et al.*, "5G field experimental trial on frequency domain multiplexing of mixed numerology," in *Proc. IEEE 85th Veh. Technol. Conf. (VTC Spring)*, Jun. 2017, pp. 1–5.
[28] L. Zhang, A. Ijaz, P. Xiao, M. M. Molu, and R. Tafazolli, "Filtered OFDM systems, algorithms, and performance analysis for 5G and beyond," *IEEE Trans. Commun.*, vol. 66, no. 3, pp. 1205–1218, Mar. 2018.
[29] J. Wen, J. Hua, W. Lu, Y. Zhang, and D. Wang, "Design of waveform shaping filter in the UFMC system," *IEEE Access*, vol. 6, pp. 32300–32309, 2018.
[30] Z. Zhang, H. Wang, G. Yu, Y. Zhang, and X. Wang, "Universal filtered multi-carrier transmission with adaptive active interference cancellation," *IEEE Trans. Commun.*, vol. 65, no. 6, pp. 2554–2567, Jun. 2017.
[31] P. Weitkemper, J. Bazzi, K. Kusume, A. Benjebbour, and Y. Kishiyama, "On regular resource grid for filtered OFDM," *IEEE Commun. Lett.*, vol. 20, no. 12, pp. 2486–2489, Dec. 2016.
[32] P. Weitkemper, J. Bazzi, K. Kusume, A. Benjebbour, and Y. Kishiyama, "Adaptive filtered OFDM with regular resource grid," in *Proc. IEEE Int. Conf. Commun. Workshops (ICC)*, May 2016, pp. 462–467.
[33] X. Cheng, Y. He, B. Ge, and C. He, "A filtered OFDM using FIR filter based on window function method," in *Proc. IEEE 83rd Veh. Technol. Conf.*, May 2016, pp. 1–5.
[34] Y.-P. Lin and P. P. Vaidyanathan, "A Kaiser window approach for the design of prototype filters of cosine modulated filterbanks," *IEEE Signal Process. Lett.*, vol. 5, no. 6, pp. 132–134, Jun. 1998.
[35] F. J. Harris, "On the use of windows for harmonic analysis with the discrete Fourier transform," *Proc. IEEE*, vol. 66, no. 1, pp. 51–83, Jan. 1978.
[36] J. Kaiser and R. Schafer, "On the use of the I_0-sinh window for spectrum analysis," *IEEE Trans. Acoust., Speech, Signal Process.*, vol. 28, no. 1, pp. 105–107, Feb. 1980.
[37] A. Goldsmith, *Wireless Communications*. Cambridge, U.K.: Cambridge Univ. Press, 2005.
[38] K. C. Hu and A. G. Armada, "SINR analysis of OFDM and f-OFDM for machine type communications," in *Proc. IEEE 27th Annu. Int. Symp. Pers., Indoor, Mobile Radio Commun. (PIMRC)*, Sep. 2016, pp. 1–6.
[39] S. Chen and C. Zhu, "ICI and ISI analysis and mitigation for OFDM systems with insufficient cyclic prefix in time-varying channels," *IEEE Trans. Consum. Electron.*, vol. 50, no. 1, pp. 78–83, Feb. 2004.
[40] K. Cho and D. Yoon, "On the general BER expression of one-and two-dimensional amplitude modulations," *IEEE Trans. Commun.*, vol. 50, no. 7, pp. 1074–1080, Jul. 2002.
[41] M. R. D. Zadeh, M. Fathian, and M. R. Gholamian, "A new method for clustering based on development of imperialist competitive algorithm," *China Commun.*, vol. 11, no. 12, pp. 54–61, Dec. 2014.
[42] M. Khosravi, M. Banejad, and H. T. Shandiz, "Robust dynamic state estimation of power system using imperialist competitive algorithm," *Can. J. Elect. Comput. Eng.*, vol. 41, no. 2, pp. 64–76, 2018.

MEIJIE YANG received the B.S. degree from the University of Science and Technology Beijing, China, in 2016, where she is currently pursuing the Ph.D. degree. Her research interests mostly include physical layer, advanced waveforms techniques, and signal processing for 5G systems.

YUEYUN CHEN received the bachelor's degree from the South China University of Technology and the master's and Ph.D. degrees from Beijing Jiaotong University. She is currently a Professor with the School of Computer and Communication Engineering, University of Science and Technology Beijing, China. Her current research interests include wireless and mobile communications, including MIMO, communication signal processing, radio resource management, cognitive radio, cooperative communications, and optimization theory on communications.

LIPING DU received the B.E. degree in industrial automation and the M.Sc. degree in physical science and technology from Zhengzhou University, Zhengzhou, China, in 1998 and 2001, respectively, and the Ph.D. degree in electronic engineering from the Beijing Institute of Technology, Beijing, China, in 2005. From 2005 to 2007, she was a Senior Research Associate with the City University of Hong Kong, Hong Kong. She is currently an Associate Professor with the University of Science and Technology Beijing. Her current research interests include signal processing, image processing, and bioinformatics.